Supplement of Atmos. Chem. Phys., 18, 12953–12967, 2018
https://doi.org/10.5194/acp-18-12953-2018-supplement

Atmospheric Chemistry and Physics
Open Access
EGU

Supplement of

Intermittent turbulence contributes to vertical dispersion of $PM_{2.5}$ in the North China Plain: cases from Tianjin

Wei Wei et al.

Correspondence to: Hongsheng Zhang (hsdq@pku.edu.cn)

In order to elaborate the details of the arbitrary-order Hilbert spectral analysis (arbitrary-order HSA), vertical wind-speed observed on 6 December 2016 is randomly taken as an example. Firstly, the 30-min vertical wind-speed fluctuation X(t) is broken down into 13 intrinsic mode functions $C_i(t)$ and one residual $r_n(t)$ using empirical mode decomposition. In this way, X(t) can be written as $X(t) = \sum_{i=1}^{n} C_i(t) + r_n(t)$, where $r_n(t)$ is a monotonic function and each $C_i(t)$ meets the two conditions of intrinsic mode functions. In the case of Figure 1S, we got 13 intrinsic mode functions and one residual. According to Huang et al. (1998), an intrinsic mode function is a function satisfying: (i) the difference between the number of local extrema and the number of zero-crossings must be zero or one, and (ii) the running mean values of the envelope defined by the local maxima and the envelope defined by the local minima are zero. That is, the intrinsic mode function in each cycle, defined by the zero crossings, involves only one mode of oscillation, which means that each intrinsic mode function is a 'monocomponent' signal. Based on this, the Hilbert transform (Cohen, 1995) can be applied to each intrinsic mode function to extract the instantaneous information (i.e. instantaneous frequency and amplitude).

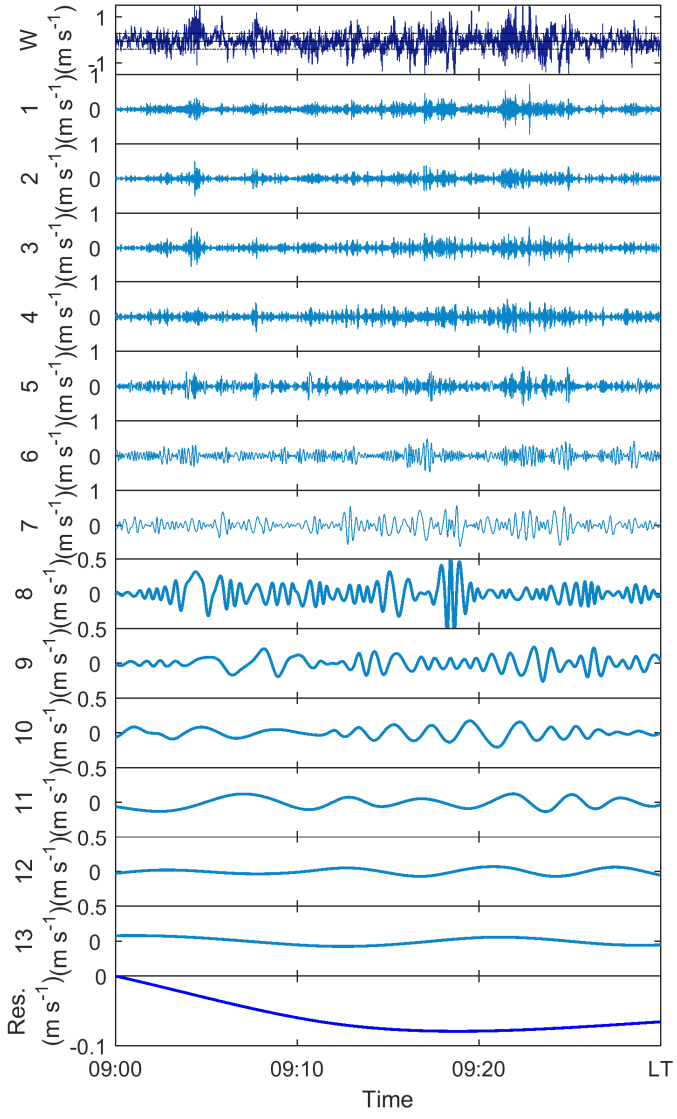

Figure S1. Results of empirical mode decomposition: original vertical wind-speed fluctuation (the black full line and dotted lines are the mean and standard deviation), modes 1–14 and the residual. Take

09:00—09:30 LT, 6 December 2016 as an example.

Using Hilbert transform, the analytical signal of $C_i(t)$ can be developed as $C_i^A(\mathrm{t}) = C_i(t) + j\tilde{C}_i(t) = A_i(t)\exp(j\theta_i(t))$, where $A_i(t)$ and $\theta_i(t)$ are the instantaneous amplitude and phase. Then the instantaneous frequency also can be defined as $\omega_i(t) = \frac{1}{2\pi}\frac{d\theta_i}{dt}$. Based on the instantaneous frequency $\omega_i(t)$ and amplitude $A_i(t)$, one can define the joint probability density function (p.d.f.) $\mathrm{p}(\omega, A)$. Further, the arbitrary-order Hilbert spectrum can be established as $\mathcal{L}_q(\omega) = \int \mathrm{p}(\omega, A)A^q dA$, where $q \geq 0$ is the arbitrary moment. Figure 2S shows an example of the joint p.d.f. $\mathrm{p(A, f)}$ and Figure S3 illustrates the arbitary-order Hilbert spectra from $q = 0$ to $q = 4$. The choice of q_{max} considers the compromise between computing efficiency and accuracy in the measurements of high-order moments (Frisch, 1995). The higher the order is, the longer the length of sample is required, while the longer data cost much more computing resource when applying arbitrary-order HSA. Hence, $q_{max} = 4$ is adopted in this study. In particular, given that the square of amplitude is equivalent to energy density, the second-order Hilbert spectrum $\mathcal{L}_2(\omega)$ can be an analogical representation of classic Fourier energy spectrum.

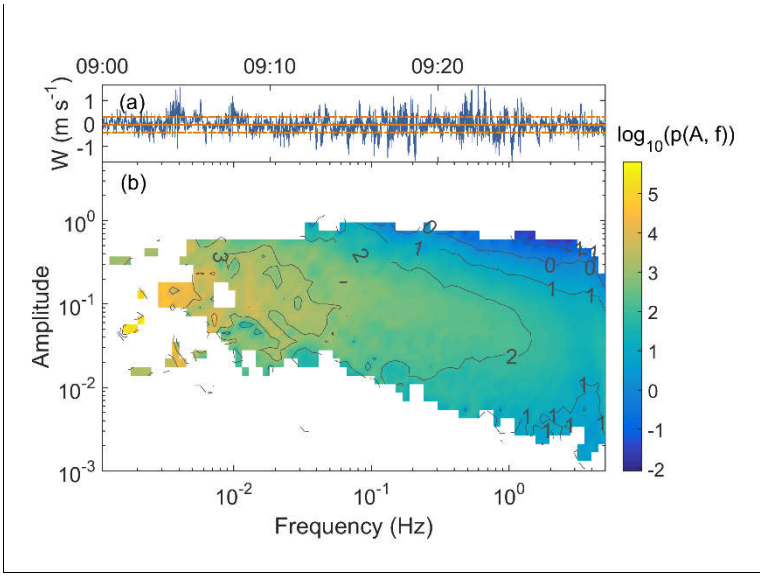

Figure S2. Representation of a joint p.d.f. $\mathrm{p(A, f)}$ as a log-log plot, the same case as in Fig. S1

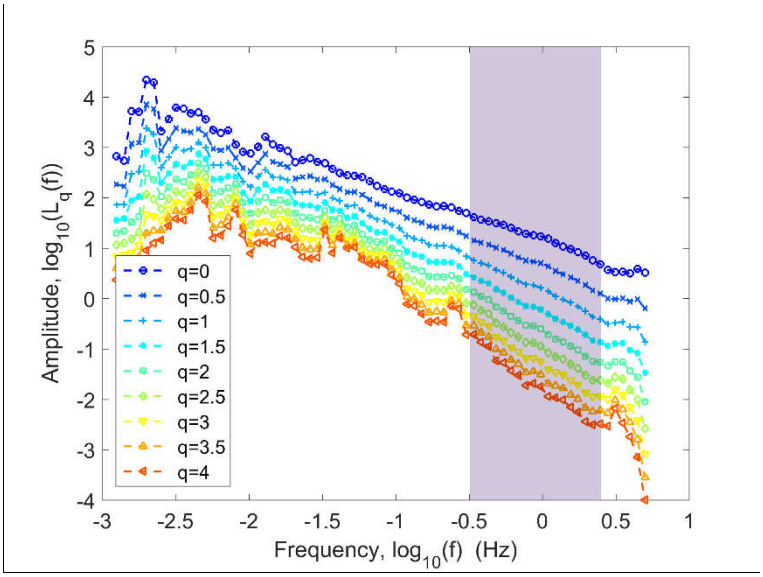

Figure S3. Arbitary-order Hilbert spectra, where order $q \leq 4$, the same case as in Fig. S1. The shaded area delineates the inertial subrange.

One noticeable feature in Figure S3 is the scale invariance in the inertial subrange, where the arbitrary-order Hilbert spectrum meets $\mathcal{L}_q(\omega) \sim \omega^{-\xi(q)}$, where ω is the frequency and $\xi(q)$ is the scaling exponent function. In the process of arbitrary-order HSA, the inertial subrange is estimated according to the distribution of $\mathcal{L}_3(\omega)$. Conventionally, the scaling exponent function $\zeta(q)$ is applied into the analyses of intermittency (Kolmogorov 1941, 1962), where $\zeta(q)$ is the scaling exponent function derived from the structure function $S_q(l) = \langle(\delta X(l))^q\rangle = \langle(X(l+l_0) - X(l_0))^q\rangle \sim l^{\zeta(q)}$. If the turbulence is fully developed and follows the Kolmogorov's theory, the distribution of scaling exponent function with the order q is linear and meets $\zeta(q) = q/3$. Dimensional analysis (Huang et al. 2008, 2011; Huang 2009) leads to $\xi(q) = \zeta(q) + 1$. Figure S4 gives the Hilbert-based scaling exponent function $\xi(q) - 1$ compared with the theoretical $\xi(q) - 1 = q/3$. Since $\xi(q) - 1 = q/3$ represents fully-developed turbulence, the deviation from $q/3$ manifests the degree of intermittency in the turbulence. In order to quantify the discrepancy of concave curves in Figure S4, the Intermittent Factor (IF) was proposed as the deviation from the theoretical value at the maximal order, that is, $\mathrm{IF} = \xi(q_{max}) - 1 - q_{max}/3$. Figure S5 shows the corresponding distribution of IF values.

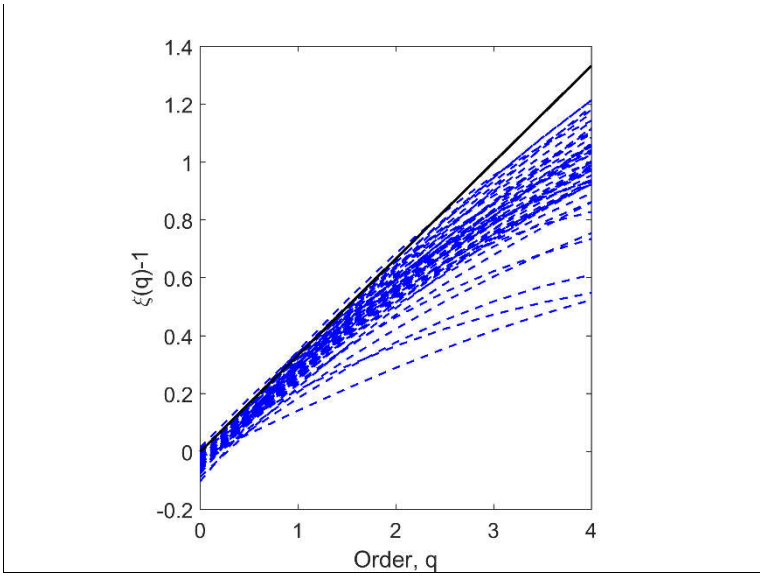

Figure S4. Representation of the Hilbert-based scaling exponent function $\xi(q) - 1$ on 6 December 2016. Black line stands for $\xi(q) - 1 = q/3$

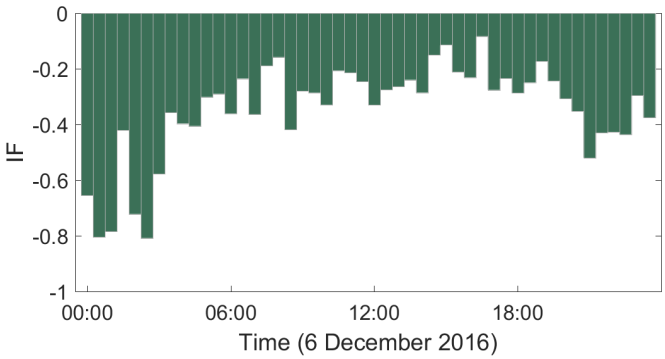

Figure S5. Distribution of $\mathrm{IF} = \xi(q_{max}) - 1 - q_{max}/3$ on 6 December 2016.

Figure S1–S5 illustrate the process of the arbitrary-order HSA. Figure S6 gives a flowchart of the method. The reason why the arbitrary-order HSA is applied to this work is that this method is more suitable for the analyses of nonlinear and non-stationary turbulent signals, compared with traditional techniques, such as Fourier analysis and Wavelet transform. It is known that, the data, whether from physical measurements or numerical modeling, most likely will have some problems: (a) the total data span is too short; (b) the data are non-stationary; and (c) the data represent nonlinear processes. While the Fourier analysis has some crucial restrictions: the system should be linear; and the data should be strictly periodic or stationary; otherwise, the resulting spectrum will make little physical sense. However, for lack of alternatives, Fourier spectral analysis is still applied to many kinds of data which may result in misleading results. On the other hand, the wavelet approach is essentially an adjustable window Fourier spectral analysis, with the basic wavelet function that satisfies certain very general conditions. As the traditional technique for the analysis of intermittency, the structure function is essentially associated with the Fourier decomposition, which means that the scaling exponent function $\zeta(q)$ has some limitations in the application of nonlinear and non-stationary turbulence signals.

As discussed by Huang et al. (1998, 1999), the arbitrary-order HSA technique is intuitive, direct,

and adaptive, with a posteriori-defined basis, from the decomposition method, based on and derived from the data, it is more appropriate for the analysis of nonlinear and non-stationary turbulence signals. Since its introduction, the HSA method has been successfully applied into different fields, including climatology (Molla et al. 2006; Hu et al. 2014), meteorology (Karipot et al. 2009; Vincent et al. 2011) and oceanography (Chen et al. 2014), to name just a few. One of the authors (Wei et al. 2017) used arbitrary-order HSA technique to separate fine-scale and large-scale motions in the stable boundary layer (SBL) and obtained a better approximation to the Monin-Obukhov similarity theory than using bandpass filtering method. Bases on these considerations and previous work, we believe that the arbitrary-order HSA technique is a suitable method for the study of turbulence intermittency in the SBL.

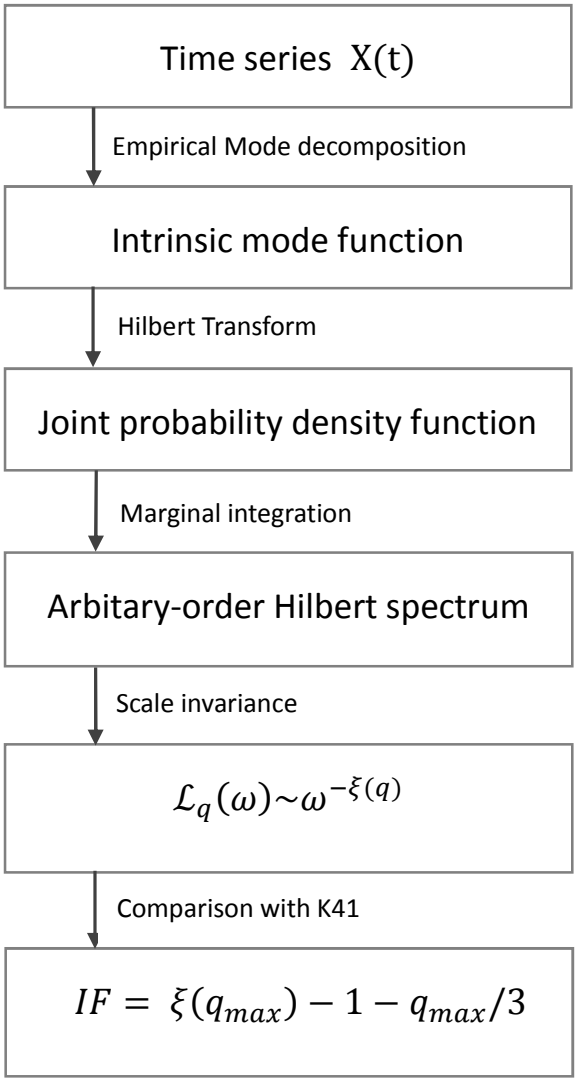

Figure S6. Schematic of arbitrary-order Hilbert spectrum analysis

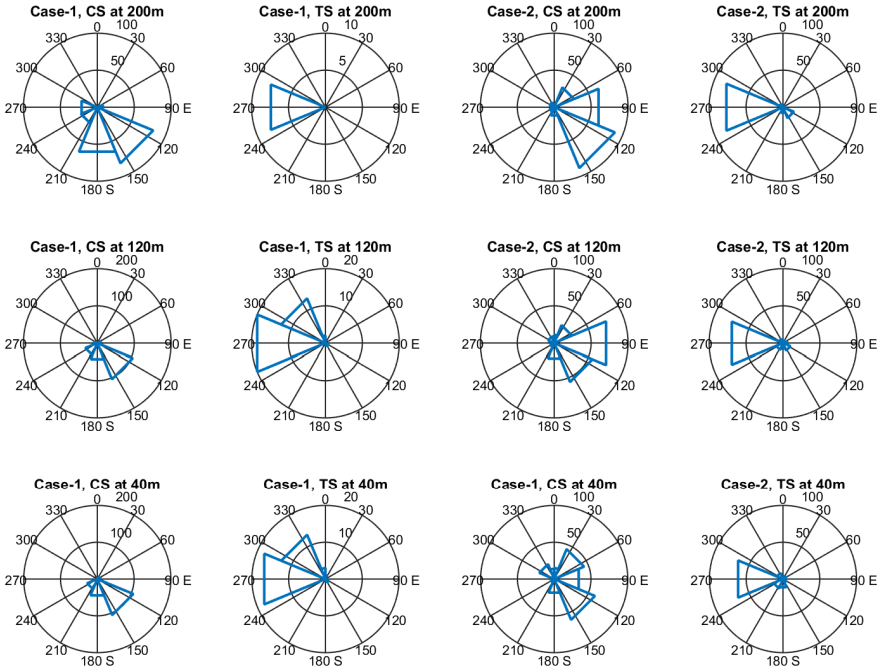

Figure S7. Comparison of rose diagram between the CS and the TS for two cases at three levels.

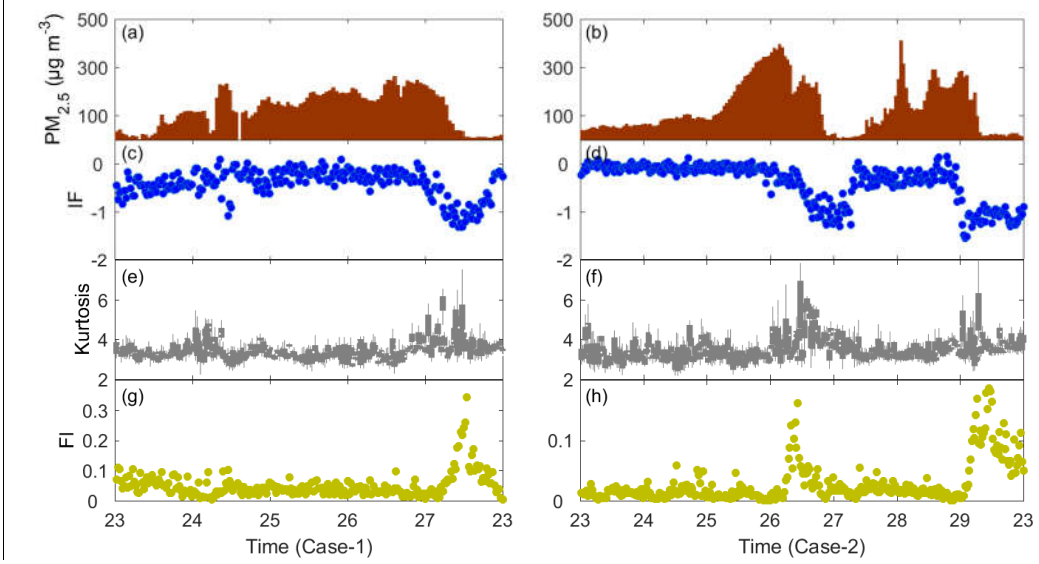

Figure S8. Comparison between PM2.5 concentration and different indexes for turbulent intermittency: **(a)** – **(b)** PM2.5 concentration; **(c)** – **(d)** IF; **(e)** – **(f)** kurtosis at a scale of 10 min; and **(g)** – **(h)** FI by Mahrt (1998). The left panel is for Case-1 and the right panel is for Case-2.

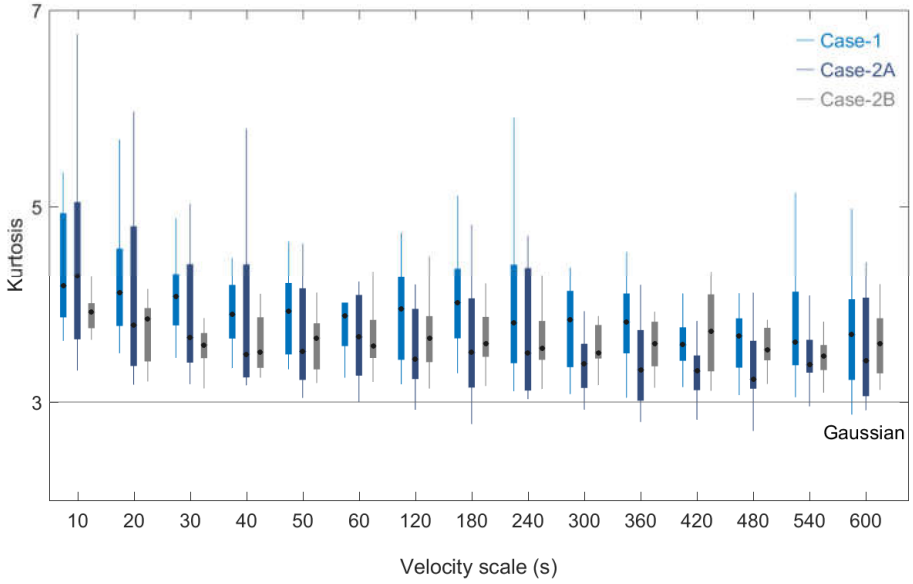

Figure S9. Kurtosis of vertical velocity increments at different scales (10 – 600 s). For each whisker diagram, the central rectangle spans the first quartile to the third quartile; the segment inside the rectangle shows the median and "whiskers" above and below the box show the locations of the minimum and maximum. The grey solid line denotes the Gaussian value. All of the data are from 00:00–06:00 LT (local time) on 27 Dec (Case-1), 26 Jan (Case-2A), and 29 Jan (Case-2B).

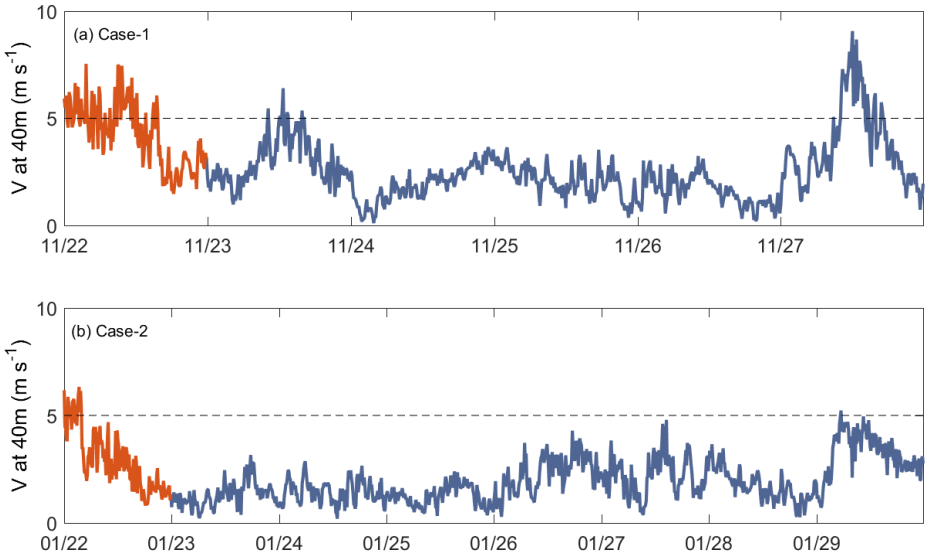

Figure S10. 10-min averaged horizontal wind speed V at 40 m for **(a)** Case-1 and **(b)** Case-2. The orange solid line represents the extra data on 22 Dec, 2016 and 22 Jan, 2017. The dashed black line marks the suggested threshold value (5 m s^{-1}).

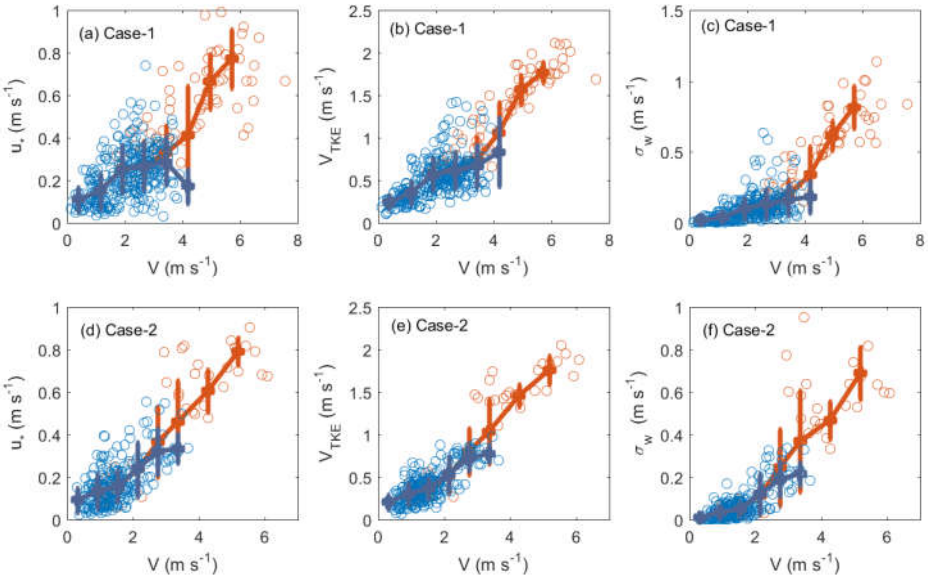

Figure S11. The relationship between the friction velocity u_*, turbulence strength $V_{TKE} = \sqrt{(\sigma_u^2 + \sigma_v^2 + \sigma_w^2)/2} = \sqrt{TKE}$ (Sun et al., 2012), standard deviation of the wind speed σ_w, and horizontal wind speed V at 40 m during the nighttime. The blue plot represents samples from the pollution cases and the orange plot is based on the extra data on the night of 22 Dec, 2016 and 22 Jan, 2017. The errorbar denotes the bin-averaged results. The top panel is for Case-1 and bottom panel is for Case-2.

References

Chen, J., Zhang, R., Wang, H., Li, J., Hong, M., & Li, X. (2014). Decadal modes of sea surface salinity and the water cycle in the tropical Pacific Ocean: The anomalous late 1990s. Deep Sea Research Part I: Oceanographic Research Papers, 84, 38-49.

Cohen, L. (1995). Time-frequency analysis (Vol. 778). Prentice hall, Englewood Cliffs, NJ.

Frisch, U. (1995). Turbulence: the legacy of AN Kolmogorov. Cambridge university press, Great Britain.

Hu, W., Biswas, A., & Si, B. C. (2014). Application of multivariate empirical mode decomposition for revealing scale-and season-specific time stability of soil water storage. Catena, 113, 377-385.

Huang, N. E., Shen, Z., & Long, S. R. (1999). A new view of nonlinear water waves: the Hilbert spectrum. Annual review of fluid mechanics, 31(1), 417-457.

Huang, N. E., Shen, Z., Long, S. R., Wu, M. C., Shih, H. H., Zheng, Q., ... & Liu, H. H. (1998). The empirical mode decomposition and the Hilbert spectrum for nonlinear and non-stationary time series analysis. In Proceedings of the Royal Society of London A: mathematical, physical and engineering sciences, 454(1971), 903-995.

Huang, Y. X., Schmitt, F. G., Hermand, J. P., Gagne, Y., Lu, Z. M., & Liu, Y. L. (2011). Arbitrary-order Hilbert spectral analysis for time series possessing scaling statistics: comparison study with detrended fluctuation analysis and wavelet leaders. Physical Review E, 84(1), 016208.

Huang, Y. X., Schmitt, F. G., Lu, Z. M., & Liu, Y. L. (2008). An amplitude-frequency study of turbulent scaling intermittency using empirical mode decomposition and Hilbert spectral analysis. EPL

(Europhysics Letters), 84(4), 40010.

Huang, Y., Schmitt, F. G., Lu, Z., & Liu, Y. (2009). Analysis of daily river flow fluctuations using empirical mode decomposition and arbitrary order Hilbert spectral analysis. Journal of Hydrology, 373(1-2), 103-111.

Karipot, A., Leclerc, M. Y., & Zhang, G. (2009). Characteristics of nocturnal low-level jets observed in the north Florida area. Monthly Weather Review, 137(8), 2605-2621.

Kolmogorov, A. N. (1941). The local structure of turbulence in incompressible viscous fluid for very large Reynolds numbers. In Dokl. Akad. Nauk SSSR, 30(4), 299-303.

Kolmogorov, A. N. (1962). A refinement of previous hypotheses concerning the local structure of turbulence in a viscous incompressible fluid at high Reynolds number. Journal of Fluid Mechanics, 13(1), 82-85.

Molla, M., Islam, K., Rahman, M. S., Sumi, A., & Banik, P. (2006). Empirical mode decomposition analysis of climate changes with special reference to rainfall data. Discrete dynamics in Nature and Society, 2006.

Sun, J., Mahrt, L., Banta, R. M., & Pichugina, Y. L. (2012). Turbulence regimes and turbulence intermittency in the stable boundary layer during CASES-99. Journal of the Atmospheric Sciences, 69(1), 338-351.

Vincent, C. L., Pinson, P., & Giebela, G. (2011). Wind fluctuations over the North Sea. International Journal of Climatology, 31(11), 1584-1595.

Wei, W., Zhang, H. S., Schmitt, F. G., Huang, Y. X., Cai, X. H., Song, Y., ... & Zhang, H. (2017). Investigation of Turbulence behaviour in the stable boundary layer using arbitrary-order Hilbert spectra. Boundary-Layer Meteorology, 163(2), 311-326.